CrossMark

RESEARCH PAPER

On-chip fabrication and magnetic force estimation of peapod-like hybrid microfibers using a microfluidic device

**Tao Sun · Chengzhi Hu · Masahiro Nakajima ·
Masaru Takeuchi · Minoru Seki · Tao Yue ·
Qing Shi · Toshio Fukuda · Qiang Huang**

Abstract Combining microfluidic methods for generating microdroplets and spinning microfibers, a novel type of alginate hybrid microfiber encapsulating different microdroplets is fabricated for various applications such as cell culture, tissue engineering and drug release. Traditional fabrication methods mainly depend on the microfluidic structure, so an effective method that uses microfluidic solution flow rates to control the generation of hybrid microfibers has not yet been developed. In this paper, we fabricate a microfluidic flow-focusing device with a long gelation microchannel to encapsulate magnetic oil microdroplets (MOMs) into alginate microfibers. We establish a hybrid microfiber generation model for this fabrication method based on limited flow rate to control microfiber width, MOM diameter and the distance between consecutive MOMs. We also calculate the magnetic force acting on a single MOM by measuring the distance and the MOM is deflected by disk magnets with respect to time in the long gelation microchannel. The magnetic forces acting on the microfibers can be further calculated by counting the number of encapsulated MOMs. The developed method has great potential for quantitative

fabrication of diverse hybrid microfibers encapsulating a variety of magnetic hydrophobic microdroplets with estimated magnetic forces. Such magnetic hybrid microfibers are attractive for use in higher order alginate microfiber assemblies and dual drug delivery systems.

Keywords Microfluidic flow-focusing device · Gelation microchannel · Magnetic microfibers · Microfiber generation model · Magnetic force estimation

1 Introduction

Microfluidic devices are a novel tool to control fluid at the microscale, and homogenous microdroplets and hydrogel-based microfibers can be formed in them (Atencia and Beebe 2005). On the one hand, a large amount of microdroplets with different materials, structures and shapes have been fabricated in diverse microfluidic devices (Christopher and Anna 2007; Vladisavljević et al. 2012). The boundary of the microdroplet provides a protective layer to prevent the materials encapsulated in the microdroplet mixing with the external environment. Thus, microdroplets can be used as microcarriers for drug delivery (Yang et al. 2009a, b) and microcapsules for cell culture (Agarwal et al. 2013). On the other hand, as popular microfluidic-spun microfibers, alginate hydrogel microfibers are a well-established scaffold for cell culture because of their high biocompatibility, high porosity and low toxicity. Alginate microfibers with a variety of morphologies, including solid (Shin et al. 2007), flat (Yamada et al. 2012), grooves (Kang et al. 2012) and hybrid (Kang et al. 2011) have been produced using a variety of methods. However, these methods are limited by the use of one type of base material. It remains a challenge to fabricate alginate hybrid microfibers with multiple

T. Sun · Q. Shi (✉) · T. Fukuda · Q. Huang
Intelligent Robotics Institute, School of Mechatronical
Engineering, Beijing Institute of Technology,
5 South Zhongguancun Street, Haidian District,
Beijing 100081, China
e-mail: shiqing@bit.edu.cn

C. Hu · M. Nakajima · M. Takeuchi · T. Yue
Department of Micro-Nano Systems Engineering,
Nagoya University, Furo-cho, Chikusa-ku, Nagoya,
Aichi 464-8603, Japan

M. Seki
Department of Applied Chemistry and Bioengineering,
Chiba University, 1-33, Yayoi-cho, Inage-ku,
Chiba 263-8522, Japan

materials. Such materials may exhibit flexible functionalities for new applications.

Recently, two microfluidic methods have been used to fabricate some novel hybrid alginate microfibers by embedding microdroplets with different materials. Alginate microfibers containing gas bubbles have been fabricated by injecting gas from an air microchannel into an alginate solution microchannel (Kang et al. 2011). A pneumatic valve was mounted on an air microchannel to generate gas bubbles with periodic or uniform distribution throughout the microfiber. The gas bubbles could temporarily provide oxygen to encapsulated cells. Hybrid microfibers encapsulating gas bubbles with uniform distribution can be also fabricated by another simpler microfluidic method. Specifically, alginate flow containing gas bubbles can be generated in microfluidic T-junction or flow-focusing junctions where alginate solution and gas merge, and then, the gas bubbles can be fixed into the alginate microfiber through cross-linking reaction. Using this method, bamboo-like alginate hybrid microfibers containing poly (lactic-co-glycolic acid) (PGLA)-dimethyl carbonate (DMC) microdroplets have been produced as dual delivery carrier (Yu et al. 2014). However, the alginate flow was cross-linked in $CaCl_2$ solution, which made the microfiber diameter mainly depend on the size of the microfluidic spinning orifice. Therefore, we consider, it is necessary to develop an effective method that depends on microfluidic solution flow rates to generate hybrid microfibers with controlled structures.

The poor controllability of hydrogels limits their use in the fabrication of 3D tissue constructs and accurate targeting in mass delivery (Li et al. 2013). Recently, diverse microscale hydrogels with Fe_3O_4 magnetic nanoparticles have been fabricated to increase their controllability for drug release (Hanuš et al. 2013) and 3D hydrogel assembly (Xu et al. 2011). Fe_3O_4 magnetic nanoparticles have the advantages of superparamagnetism and high saturation field, and they can be stabilized in polar or nonpolar suspensions using modified surfactants (Yang et al. 2009a, b). Fe_3O_4 magnetic nanoparticles have been directly incorporated into alginate fibers, facilitating the rapid response of the generated fibers to an external magnetic field. This magnetic controllability allows alginate fibers to be used in applications such as single cell manipulation (Liu et al. 2012), 3D alginate fiber assembly (Hu et al. 2013) and controlled drug release (Lin et al. 2012). However, it is difficult to measure the magnetic forces acting on magnetic fibers. This hinders the precise manipulation of magnetic microfibers.

In this paper, we use a microfluidic flow-focusing device with a long gelation microchannel to fabricate alginate hybrid microfibers encapsulating magnetic oil microdroplets (MOMs) with uniform distribution. After detailed analysis of the synthesis of these hybrid microfibers, we establish a hybrid microfiber generation model based on limited flow rate. This model is then used to generate

hybrid microfibers with the desired microfiber width, MOM diameter and distance between consecutive MOMs, which allows the easy and precise adjustment of the concentration of magnetic nanoparticles in the microfiber fabrication process. Furthermore, we could calculate the magnetic force acting on each MOM by measuring the deflection distance of MOM induced by an external magnet with respect to time in the gelation microchannel. Using a theoretical model (Zhang et al. 2009), we could also estimate the magnetic force acting on MOMs with different diameters in various magnetic fields. Each MOM could be represented as a controlled unit, so the magnetic forces acting on each microfiber could be calculated by counting the number of encapsulated MOMs. The developed method allows simple fabrication of hybrid microfibers with diverse structures only depending on microfluidic solution flow rate. The estimated magnetic forces of the generated microfibers means these fibers show promise for use in higher order alginate microfiber assemblies and dual drug delivery systems.

2 Materials and methods

2.1 Materials

Mineral oil (code 23306-84) was purchased from Nacalai Tesque in Japan, and Sodium alginate, Calcium chloride, Dextran 2000.000, Iron (III) chloride (heptahydrate 99.9 %), iron (II) sulfate (heptahydrate 99.5 %), Oleic acid and 25 % Ammonia solution were purchased from Wako pure chemical industries in Japan

2.2 Preparation of magnetic mineral oil solution

Magnetic nanoparticles were fabricated as follows: $FeCl_3$ (2.7 g) and of $FeSO_4$ (1.39 g) were mixed in pure water (100 mL) to form a homogeneous solution. The solution was heated at 80 °C and then 25 % $NH_3 \cdot H_2O$ (12 mL) was added with stirring, the speed of which determined the size of the resulting particles. Oleic acid (2 mL) was added to stabilize the iron oxide nanoparticles. An external magnetic field was applied to aggregate the nanoparticles, and the excess oleic acid was removed by washing the aggregate with ethanol. The magnetic nanoparticles were dried under vacuum. Magnetic nanoparticles (0.3 g) were dispersed in mineral oil (10 mL) in an ultrasonic bath at 40 °C for 4 h to form a uniform suspension.

2.3 Microfluidic synthesis of alginate fibers encapsulating MOMs

The polydimethylsiloxane (PDMS) microfluidic substrate was fabricated using a standard soft lithography method.

A glass cover (width: 40 mm, length: 50 mm, thickness: 0.12–0.17 mm) was bonded to the PDMS substrate by air plasma treatment at 150 J for 30 s to form a microfluidic device. The bonded microfluidic device was heated at 80 °C for 5 h. Before use, the microfluidic device was treated in air plasma at 70 J for 300 s to transform the hydrophobic PDMS surface to a hydrophilic surface to form MOMs. Figure 1 shows a schematic diagram of the microfluidic device used to fabricate magnetic hybrid microfibers. The microfluidic device is composed of four consecutive parts: (1) a flow-focusing junction to form MOMs; (2) an inlet microchannel consisting of two parts with widths of 100 and 200 µm to form a stable array of MOMs; (3) a multiphase confluence microchannel; and (4) a gelation microchannel to spin the hybrid microfibers. The height of the microchannel (h) is 150 µm.

Aqueous solutions of sodium alginate (1.8 % w/v), dextran (10 % w/v) with and without 0.5 M CaCl$_2$ were used as sample, sheath and buffer solutions, respectively. All solutions were introduced into the microfluidic device at different inlets using syringe pumps, as shown in Fig. 1. The buffer solution was used in the microfiber fabrication process. On the one hand, the buffer solution can add a thickener to the buffer/gelation solutions to balance the viscosities of the solutions; on the other hand, the buffer solution can moderate the rapid gelling speed of Ca-alginate and shield the microfiber to prevent the gelation microchannel

clogging (Yamada et al. 2012). The outlet of the microfluidic device was immersed in 0.1 M CaCl$_2$ solution loaded in a Petri dish, which enabled the alginate microfiber to extrude stably and smoothly without blocking for a long time (>10 min).
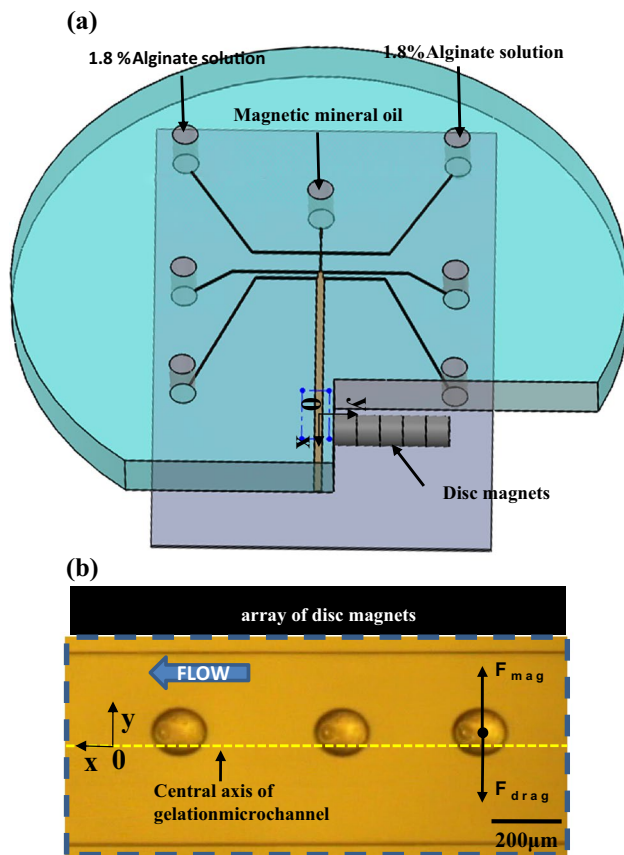
2.4 Measurement of magnetic force exerted on MOMs

The on-chip magnetic force manipulation method (Zhang et al. 2009) was used to estimate the magnetic forces acting on the MOMs. As shown in Fig. 2a, the microfluidic device was cut along the edge of the gelation microchannel, and an array of five disk magnets (diameter: 4 mm, thickness: 2 mm, magnetic flux density: $B = 300$ mT) was placed perpendicularly at the edge of the gelation microchannel. The MOMs were generated continuously at the first junction to form an array of MOMs. When the array of MOMs moved along the central axis of the gelation microchannel to pass by the disk magnets, the magnetic forces acting on the MOMs made them deflect toward the side of disk magnets, as shown in Fig. 2b. In this process, there was a drag force (F_{drag}) against the direction of magnetic force (F_{mag}) because of the relative movement between MOMs and alginate flow in the y direction. F_{drag} can be calculated from Stokes' law (Zhang et al. 2009):

$$F_{\text{drag}} = 3\pi \mu_a D V_y \tag{1}$$
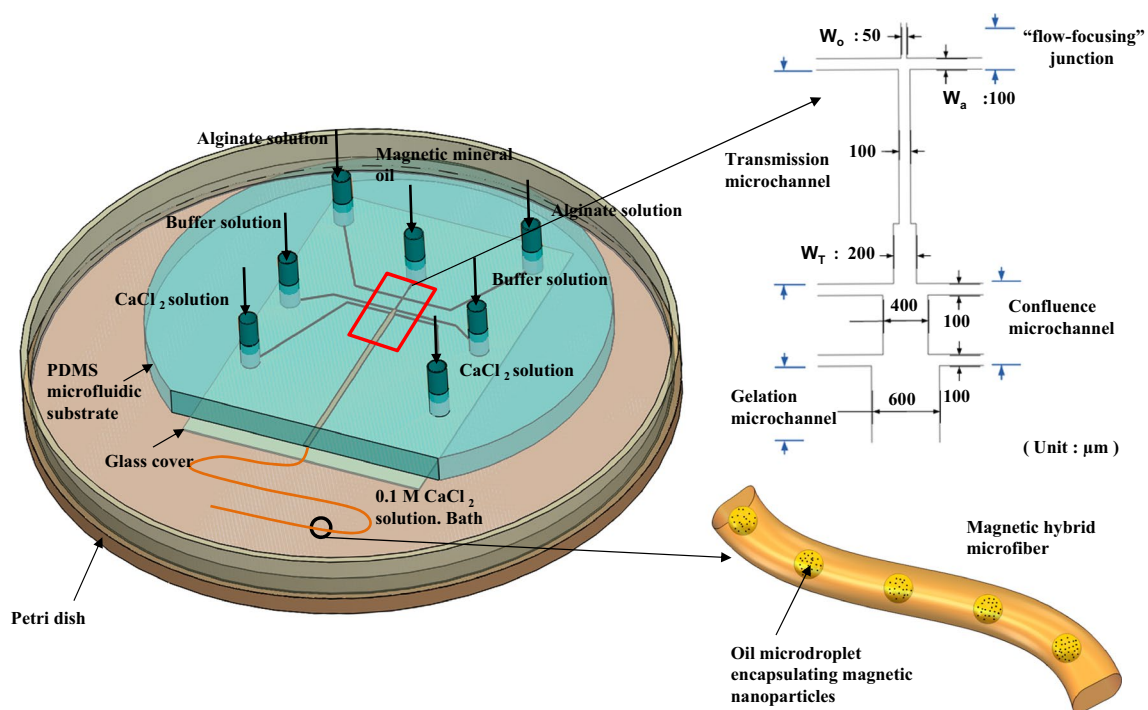
Fig. 1 Schematic illustration showing the microfluidic device used to fabricate alginate hybrid microfibers encapsulating magnetic oil microdroplets (MOMs) with uniform distribution

Fig. 2 a Design of microfluidic chip to measure the magnetic force exerted on a magnetic oil microdroplet in a specific magnetic field. **b** Inverted microscope image of deflection of magnetic oil microdroplets in the gelation microchannel

where μ_a is the kinematic viscosity of 1.8 % w/v alginate solution, which is 134 mPas; D is the diameter of the magnetic microdroplet; V_y is the velocity vector of the MOMs along the y direction. Assuming that inertia is negligible at the microscale (Suh et al. 2012), the magnetic and drag forces reach a balance, $F_{drag} = F_{mag}$. Using Eq. (1), we can calculate the magnetic forces acting on MOMs.

3 Results and discussion

3.1 Synthesis of hybrid microfibers

Controlling microfluidic interfaces in the microfluidic device, an alginate microfiber encapsulating MOMs is prepared by forming an alginate flow containing MOMs and then cross-linking the flow to form an alginate microfiber by the diffusion of Ca^{2+} ions, which simultaneously fixes the MOMs in the microfiber.

As shown in Fig. 3a, an emulsion of oil and alginate solution was formed at the first flow-focusing junction. The

hydrophilic nature of the treated microfluidic device promotes the oil solution to form microdroplets because the aqueous alginate solution preferentially interacted with the microchannel surface rather than the oil solution. An array of MOMs with uniform distribution spontaneously formed as the MOMs moved continuously along the transmission microchannel. The width of the transmission microchannel increased downstream to obtain an appropriate width of alginate flow to encapsulate the MOMs. At the second junction, the alginate flow was sandwiched by an outer buffer flow. Then, at the third junction, the outer buffer flow was encased by $CaCl_2$ solution to form multiple laminar flows. The interface between different solution flows was clearly observed, as demonstrated in Fig. 3a2.

The alginate flow then solidified to form a microfiber in the gelation microchannel. The interface between buffer and $CaCl_2$ solutions disappeared ~3 mm from the third junction. The gelled layers gradually widened to contact the array of MOMs from two sides of the alginate flow. The contact process must be sufficiently rapid to keep the array of MOMs uniform. Thus, 0.5 M $CaCl_2$ solution was chosen to achieve rapid cross-linking speed (Thomas et al. 1995). The alginate flow was transformed into a hydrogel microfiber ~1.5 cm from the third junction. Figure 3a3 shows the boundary of a microfiber appears in the buffer laminar flow, which is caused by the flat shape of the microfiber (Yamada et al. 2012). The flat shape of the hybrid microfiber is also evidenced by the bent parts of microfibers observed in Fig. 3b. The length of the gelation microchannel determines the time that the alginate solution cross-linked with $CaCl_2$ solution. If the gelation microchannel is too short, the MOMs might fall out of the alginate microfiber because of insufficient cross-linking. Conversely, if it is too long, the microchannel might be blocked by the generated microfibers. We found that a gelation microchannel with a length of 2.2 cm allowed the MOMs to be fixed tightly in the alginate microfibers without blocking the channel. Because the microfluidic outlet was immersed in the solution, each microfiber could be smoothly extruded from the microchannel, as shown in Fig. 3a4. Overall, long hybrid microfibers encapsulating uniformly distributed MOMs were fabricated by the microfluidic device. The generated microfibers resemble peapods, as shown in Fig. 3c, d.

3.2 The effect of flow rates of all solutions

In the hybrid microfibers, the MOM diameter (D), microfiber width (W) and distance between consecutive MOMs (L) are influenced by the flow rates of all of the solutions in the microchannel. In this study, three different flow rates of $CaCl_2$ solution (Q_c = 1,300, 1,500 and 1,700 μL h^{-1}) were used, and for each $CaCl_2$ solution flow rate, a range of flow rates of alginate solution (Q_a = 400, 500, 600, 700,
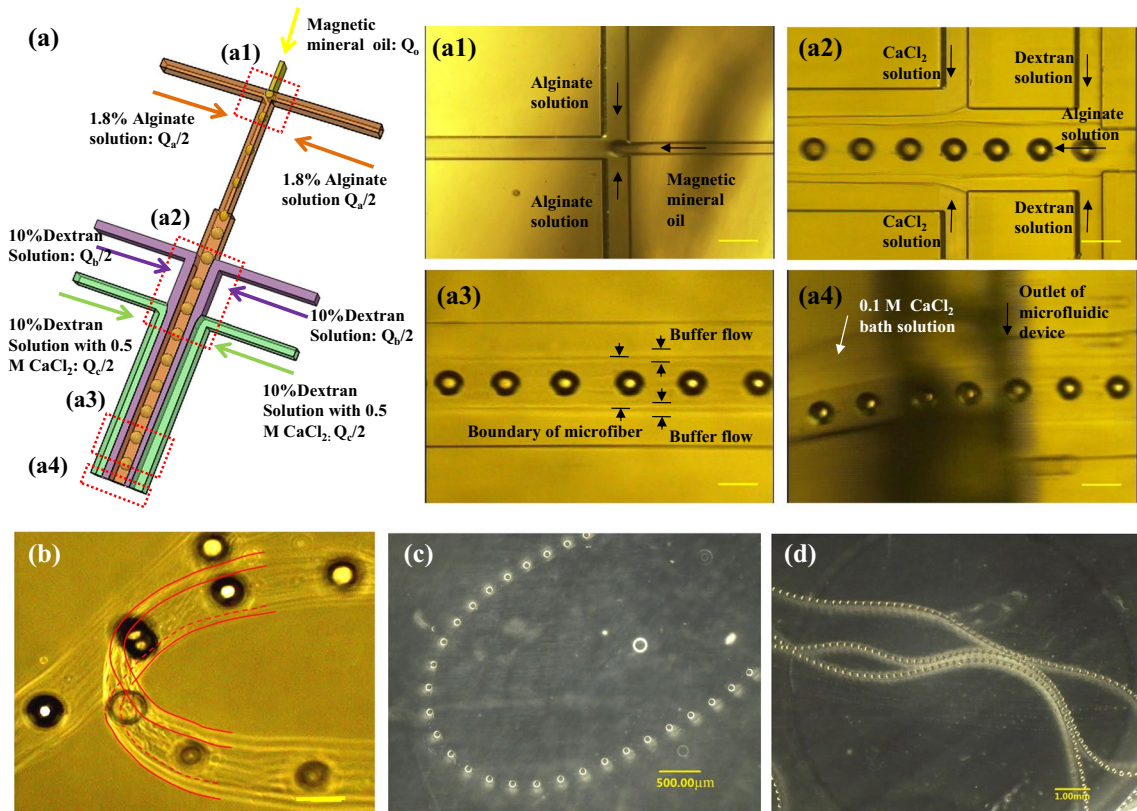
Fig. 3 a Formation of a hybrid microfiber in the microchannel. Micrographs (*a1*), (*a2*), (*a3*) and (*a4*) show microdroplet generation, confluence of all solutions, cross-linking to form a microfiber and microfiber ejection into the bath solution, respectively. **b** Opti-

cal image of bent hybrid microfiber. **c** Optical image of magnetic oil microdroplets uniformly distributed in an alginate microfiber. **d** Optical image of long hybrid microfibers. The *scale bars* in (*a1*), (*a2*), (*a3*), (*a4*), and **b** are all 200 μm

800 and 900 μL h^{-1}) was used. Furthermore, for each flow pattern of alginate and CaCl$_2$ solution, a range of flow rates of magnetic mineral oil solution (Q_o = 40, 50, 60, 70 and 80 μL h^{-1}) was investigated, this allowed us to study the effect of CaCl$_2$, alginate and oil solution flow rates on W, D and L of the hybrid microfibers. The subscripts "c", "a" and "o" denote the CaCl$_2$, alginate and oil solution, respectively. The flow rate of buffer solution was kept at 500 μL h^{-1} to fabricate uniform microfibers (Yamada et al. 2012). The observation location was ~0.5 mm from the outlet of the microfluidic device, where two boundary lines of each microfiber could be observed in the gelation microchannel. The dimensions of the MOMs generated depended on the dripping regime. Each monodisperse MOM was usually followed by a smaller satellite microdroplet, the volume of which was enough small that its influence was neglected.

Figure 4 shows a series of representative images of the hybrid alginate microfibers fabricated in the gelation microchannel, where the variation of W, D and L corresponding to different flow patterns can be observed. W decreased with a decrease of Q_a at constant Q_c or increase of Q_c at

constant Q_a. However, Q_o hardly influenced W. Figure 5a shows the average W for different oil solution flow rates as a function of Q_a at three different Q_c. Increasing Q_o leads to a much smaller distance between consecutive MOMs, but D remains nearly constant. D decreased with increasing Q_a. Keeping Q_a constant, increasing Q_c lengthens the distance between consecutive MOMs, while D remains almost constant. Figure 5b shows the average D for different Q_c and Q_o with constant Q_a. Flow rates Q_a, Q_c and Q_o all influence L, but the influence of Q_o is larger than those of Q_a and Q_c (Fig. 5c).

For a fixed Q_a, D stays nearly constant as Q_o changes. This is because the flow resistance of induced by increasing Q_o to the alginate flow is too small to measure the change of diameter of MOMs. Conversely, the higher viscous force and stronger elongation effect induced by increasing Q_a can effectively reduce the diameter of MOMs. Increasing Q_o accelerates the generation frequency of MOMs to decrease L. L can be controlled over several orders of magnitude by modifying Q_o, which enables the density of MOMs in the alginate microfibers to be controlled. For fixed Q_a and Q_o, increasing Q_c reduces the width of the alginate flow, which
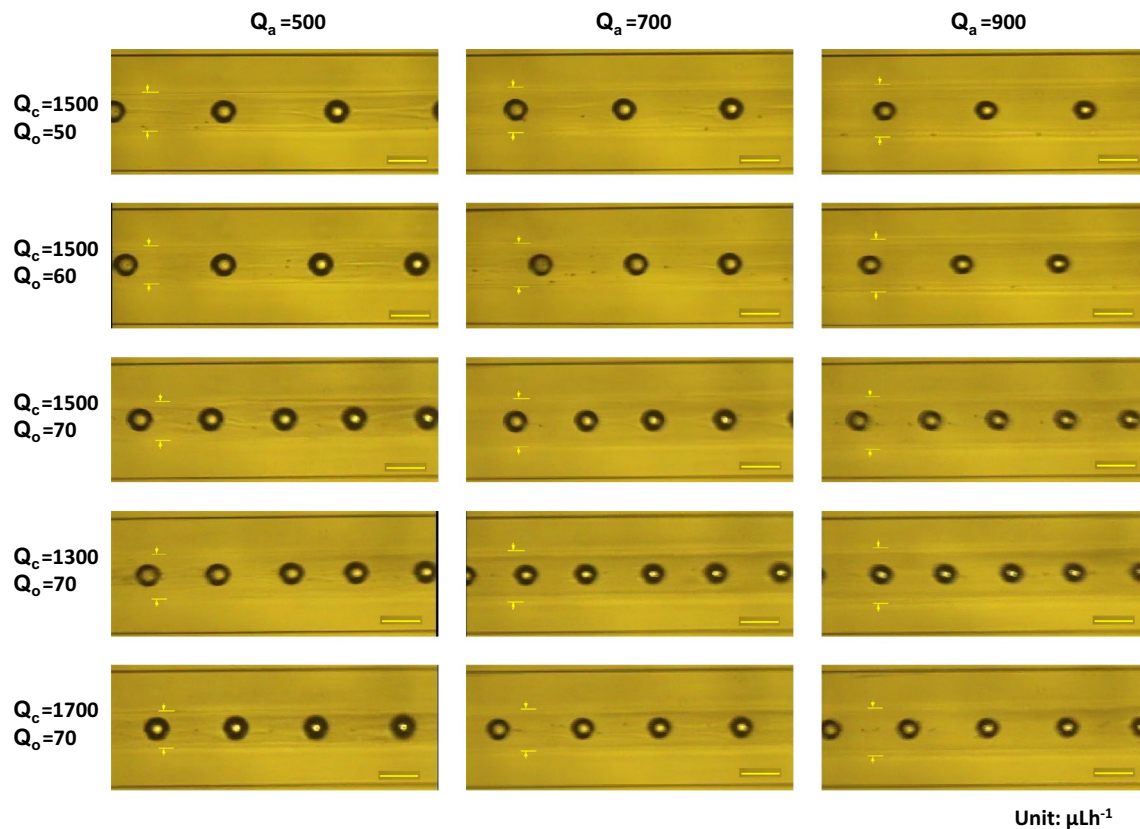
Fig. 4 Representative hybrid microfibers fabricated using different flow rate patterns. The *yellow arrows* indicate the location of microfiber boundary lines. All *scale bars* are 200 μm (color figure online)
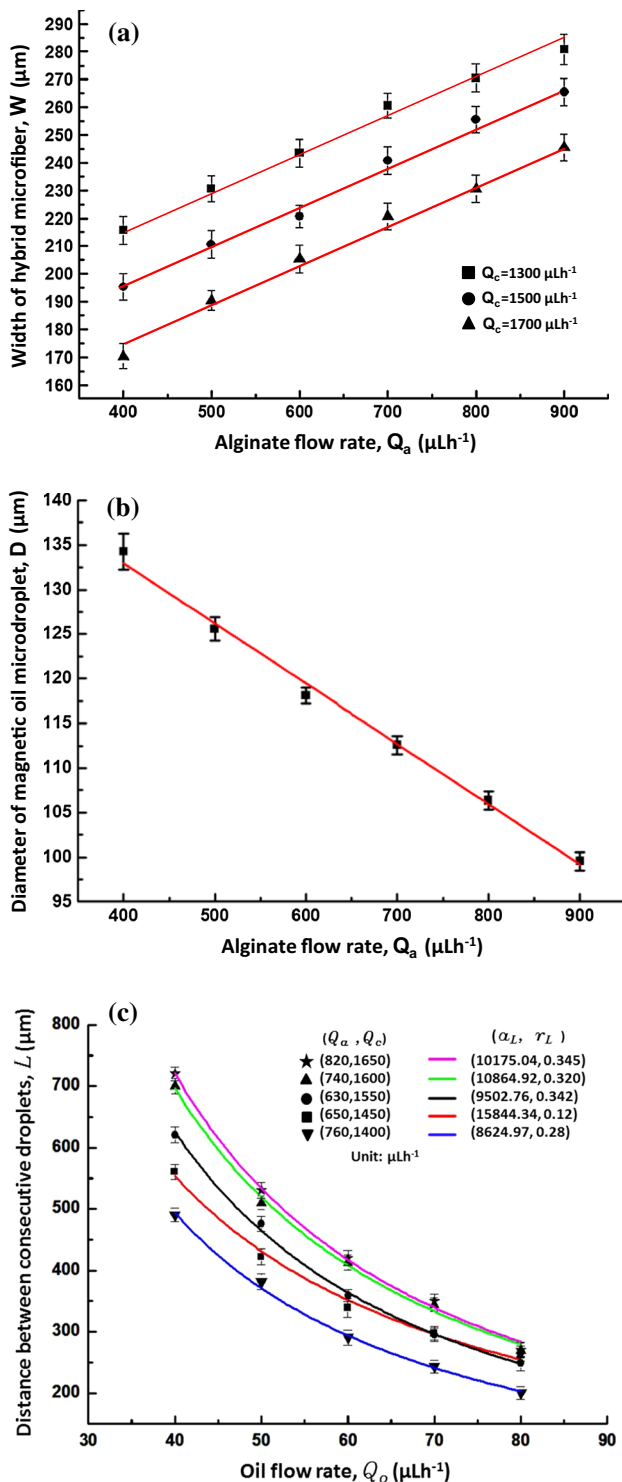
can decrease the flow resistance to MOMs transmitting in the alginate flow. As a result, L increases because the first MOM accelerates in the gelation microchannel, while the second MOM has a constant velocity in the transmission microchannel. Conversely, the increased width of alginate flow induced by decreasing Q_c can increase flow resistance to decrease L. Similar behavior has been experimentally observed in previous work (Jose and Cubaud 2012). The decreased width of alginate flow increases its velocity. The increased velocity of the alginate flow largely compensates for the effect of its decreased width on the total flow rate of alginate and oil solution through the flow-focusing junction, so the total flow resistance of alginate and oil flow in the gelation microchannel remains stable to generate MOMs with nearly constant diameters for different Q_c.

3.3 Hybrid microfiber generation model

The alginate hybrid microfibers can keep boundary and MOMs distribution uniform in limited Q_a, Q_c and Q_o. When $Q_a < 400\ \mu L\ h^{-1}$, we found the boundary of the hybrid microfiber formed a necklace-like morphology because the width of the microfiber was so narrow that the supporting influence of encapsulated MOMs appeared

(Yu et al. 2014). The microfiber width was difficult to clearly define because of the necklace-like morphology. Conversely, the width of the microfiber might be too wide to be smoothly ejected out when $Q_a > 900\ \mu L\ h^{-1}$. For $400\ \mu L\ h^{-1} \leq Q_a \leq 900\ \mu L\ h^{-1}$, the function of CaCl$_2$ flow as a lubricant to assist microfiber extrusion might be lost when $Q_c < 1{,}300\ \mu L\ h^{-1}$. In contrast, the relatively large flow rate of CaCl$_2$ solution reduced the time that alginate solution resided in the microfluidic channel, which might make MOMs unstably encapsulated because of insufficient cross-linking (Shin et al. 2007). When $Q_o > 80\ \mu L\ h^{-1}$, the array of MOMs with uniform distribution was difficult to be kept because of the close distance between consecutive MOMs (Jose and Cubaud 2012). The distance between consecutive MOMs might surpass the observed range of the inverted microscope when $Q_o < 40\ \mu L\ h^{-1}$. We thus chose $Q_a = 400$–$900\ \mu L\ h^{-1}$, $Q_c = 1{,}300$–$1{,}700\ \mu L\ h^{-1}$ and $Q_o = 40$–$80\ \mu L\ h^{-1}$ as flow rate ranges to fabricate hybrid microfibers with uniform boundaries and MOM distributions.

As shown in Fig. 5a, W is approximately proportional to Q_a for each fixed Q_c in the abovementioned ranges of flow rates, which has been experimentally observed in other alginate microfiber fabrication processes (Shin et al. 2007;

(a)

(b)

(c)

◄**Fig. 5 a** Width of hybrid microfiber versus alginate flow rate for $CaCl_2$ flow rate: Q_c. *Red lines* represent the scaling law $\frac{W}{W_T} = \frac{\alpha_w \rho_a Q_a}{2\mu_a h} - \frac{\gamma_w \rho_c Q_c}{2\mu_c h} + c_w$ determined by fitting the experimental data. Data are expressed as mean–s:d: ($n \geq 150$). **b** Diameter of magnetic oil microdroplets versus alginate flow rate. The *red line* represents the scaling law $\frac{D}{W_O} = \frac{\beta_D \mu_a Q_a}{2\sigma_{ao} W_a h} + c_D$ determined by fitting the experimental data. Data are expressed as mean–s:d: ($n \geq 150$). **c** Distance between consecutive microdroplets L versus oil flow rate Q_o for different alginate and $CaCl_2$ flow patterns. *Lines* represent the scaling law $\frac{L}{D} = \alpha_L \left(\frac{Q_a}{Q_o} \right)^{(1+\gamma_L)}$. Data are expressed as mean–s:d: ($n \geq 60$) (color figure online)

to predict W. In Eq. (2), Re_a and Re_c are the Reynolds number used to effectively describe microfluidics; $W_T = 200\ \mu m$ is the width of the downstream transmission microchannel; $\rho_a = 1.018 \times 10^3$ kg/m^3 and $\rho_c = 1.111 \times 10^3$ kg/m^3 are the densities of the solutions; $\mu_a = 134$ mPas and $\mu_c = 24$ mPas are the viscosities of the solutions; and $a_w = 99.43$, $r_w = 11.67$ and $c_w = 1.45$ are fitting parameters that are mainly dependent on the microchannel geometry (Lee et al. 2006). D is approximately proportional to Q_a, as shown in Fig. 5b. We can use the linear equation:

$$\frac{D}{W_O} = \beta_D Ca_a + c_D = \frac{\beta_D \mu_a Q_a}{2\sigma_{ao} W_a h} + c_D \qquad (3)$$

to predict D in the above-mentioned flow-rate ranges, where Ca_a is the capillary number used to describe microdroplet formation; $W_0 = 50\ \mu m$ and $W_a = 100\ \mu m$ are the width of the magnetic oil and alginate solution inlet microchannel, respectively; $\sigma_{ao} = 5.7$ mN m^{-1} is the interfacial tension; $\beta_D = 6.13$ and $c_D = 3.2$ are the fitting parameters related to the microchannel geometry (Liu and Zhang 2011). The alginate solution was used as a continuous solution in the MOM fabrication process. The approximately proportional relationship between the limited flow rate of continuous solution and diameter of generated microdroplets has also been experimentally observed previously (Miller et al. 2010). The five different flow patterns of Q_a and Q_c were matched to test scaling law Eqs. (1) and (2). The predicted and experiment results are compared in Table 1.

L is determined by the MOM generation frequency and flow resistance to MOM transmission (Thorsen et al. 2001; Jose and Cubaud 2012), both of which can be influenced by Q_a, Q_c and Q_o. However, it is difficult to find a scaling law to predict the relationships among Q_a, Q_c, Q_o and L because they are not linearly related. In this study, we first confirmed Q_a and Q_c to fix the conditions for MOM transmission and then obtained the desired L by modifying Q_o. Theoretically, any L can be obtained by varying Q_o for fixed alginate and $CaCl_2$ flow rates. Figure 5c shows the distance between consecutive MOMs as a function of Q_o for the five above-mentioned flow patterns. We found that the equation:

$$\frac{L}{D} = \alpha_L \left(\frac{Q_a}{Q_o} \right)^{(1+\gamma_L)} \qquad (4)$$

Yamada et al. 2012). Furthermore, there is also an approximately proportional relationship between W_a and Q_c for a fixed Q_a, so we can use two variable linear regression equations:

$$\frac{W}{W_T} = \alpha_w Re_a - \gamma_w Re_c + c_w = \frac{\alpha_w \rho_a Q_a}{2\mu_a h} - \frac{\gamma_w \rho_c Q_c}{2\mu_c h} + c_w \qquad (2)$$

Table 1 Comparison of predicted and experiment results for D, W and L

Flow rate (μL h^{-1})	Predicted D (μm)	Experimental D (μm)		Predicted W (μm)	Experimental W (μm)		Predicted Q_o (μL h^{-1})	Experimental L (μm)	
		Average size	RSD		Average size	RSD		Average size	RSD
$Q_a = 630$ $Q_c = 1{,}550$	117.45	117.32	0.13	222.54	225.65	2.34	67	308.23	8.34
							56	382.23	13.56
							44	450.56	11.23
$Q_a = 650$ $Q_c = 1{,}450$	112.13	112.45	0.09	235.54	232.65	1.21	64	301.34	9.12
							54	391.21	9.32
							40	473.75	14.21
$Q_a = 740$ $Q_c = 1{,}600$	108.13	107.45	0.04	251.543	253.23	3.23	73	312.79	13.54
							63	376.35	10.54
							54	471.23	12.74
$Q_a = 760$ $Q_c = 1{,}400$	108.62	108.60	0.26	256.749	254.34	2.15	59	309.29	8.45
							49	367.13	10.45
							42	459.54	12.76
$Q_a = 820$ $Q_c = 1{,}650$	104.57	103.94	0.31	239.854	240.231	3.45	76	304.23	9.35
							64	375.87	10.74
							56	465.23	12.31

Data are expressed as mean–s:d: ($n \geq 100$)

fits the data well. In Eq. (4), a_L and r_L are the fitting parameters that are mainly dependent on Ca_a and the width of alginate flow, and these parameters are different for each flow pattern. For fixed Q_a, MOMs with nearly same diameter are generated in the limited Q_o, so we can approximately take D as constant. Yu et al. (2014) observed a similar relationship between Q_o and L. For the array of MOMs generated at the first flow-focusing junction, if there is not much mass transfer and marked compressibility effects, the relationship between L and D is simply (Jose and Cubaud 2012; Sun and Cubaud 2011):

$$\frac{L}{D} = c_L \frac{Q_a}{Q_o} \qquad (5)$$

where c_L is constant. In our experiment, the width of alginate flow in the gelation microchannel was always wider than the width in the first flow-focusing junction. The wider width of the alginate flow than that of the first junction increases the flow resistance to MOM transmission, so L decreases when the MOMs flow into the gelation microchannel. For a fixed flow pattern, increasing Q_o enlarges the velocity difference between the MOMs and alginate flow, which can also increase the flow resistance to MOM transmission. The increasing flow resistance accelerates the decrease of L. A similar phenomenon was found experimentally previously (Jose and Cubaud 2012). Thus, the right item of Eq. (5) could be further multiplied by $c_1(Q_a/Q_o)^{\gamma_L}$, $(c_1 Q_a^{\gamma_L} < Q_o^{\gamma_L}, \gamma_L > 0, c_1 > 0)$ to obtain the Eq. (4). The value of $c_1 Q_a^{\gamma_L}$ should be less than that of $Q_o^{\gamma_L}$ due to the increase of flow resistance in gelation

microchannel. The acceleration on the decrease of L induced by the increasing Q_o makes the value of fitting parameter: r_L be more than zero. The fitting parameter: c_1 is constant for the fixed flow pattern. For each flow pattern, we used the corresponding scaling law equation to calculate the predicted oil flow rates for three desired distances of $L = 300$, 380 and 460 μm. These predicted oil flows were further used to check whether the experimental L agreed with the desired values. The predicted oil flow rate and experimental L are presented in Table 1.

3.4 Magnetic force acting on MOMs

A series of deflection images of a single MOM (diameter: $D = 135$ μm) was obtained with the arrangement shown in Fig. 6a. The distance from the central axis of the gelation microchannel to the center of each MOM was taken as the defection position: y. Given the initial $y = \sim 30$ μm at initial time $t = 0$, the dependence of y on t was plotted (Fig. 6b). The most suitable fit for these deflection position data is provided by the function:

$$y(t) = \alpha_y e^{\sigma_y t} + c_y \qquad (6)$$

where $a_y = 24.025$, $\sigma_y = -0.663$ and $c_y = 3.261$ are the fitting parameters. By taking the time derivative of this equation, the MOMs deflection velocity in the y direction:

$$V_y(t) = \frac{dy}{dt} = \alpha_y \sigma_y e^{\sigma_y t} \qquad (7)$$
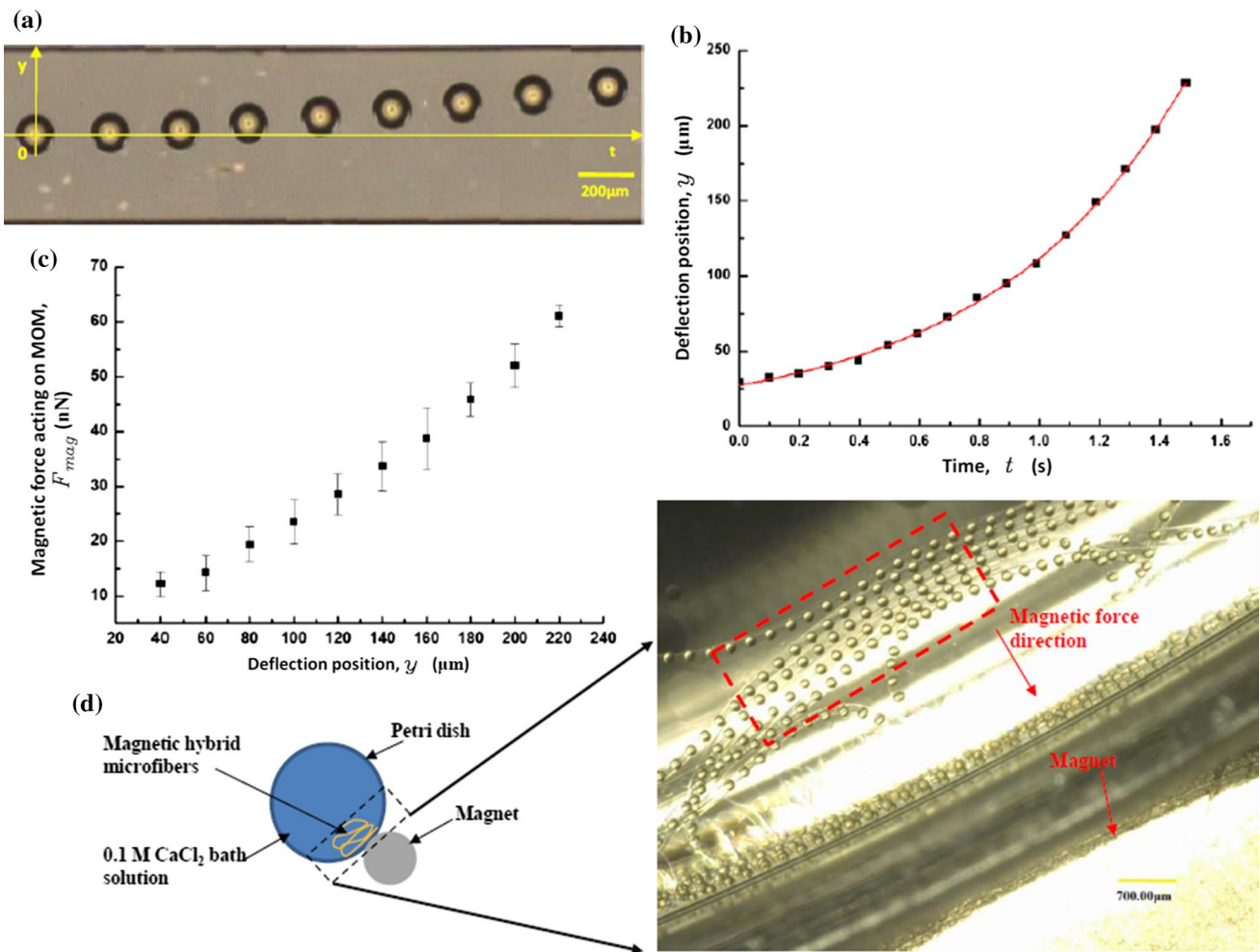
Fig. 6 **a** Photograph showing MOM deflection. **b** Typical MOM trajectory in the gelation microchannel. *Red lines* represent the scaling law $\left(y(t) = \alpha_y e^{\sigma_y t} + c_y\right)$ determined by fitting the experiment data. **c** Average magnetic force exerted on a single MOM versus deflection distance. Data are expressed as mean–s:d: ($n = 20$). **d** Photograph of multiple microfibers being induced to form a layer-by-layer assembly by a magnet (color figure online)

is obtained, allowing us to calculate the magnetic force on MOMs by combining Eq. (7) into Eq. (1):

$$F_{\text{mag}} = F_{\text{drag}} = 3\pi \mu D \alpha_y \sigma_y e^{\sigma_y t} \tag{8}$$

Using this method, the trajectories of 20 MOMs $y(t)$ were obtained, and then the average magnetic force acting on MOMs depending on deflection distance was plotted (Fig. 6c).

The theoretical magnetic force exerted on a MOM can be calculated by:

$$F_{\text{mag}} = \frac{N \Delta \chi V_{\text{P}}}{\mu_0} B(\nabla B) = \frac{2 \Delta \chi C \pi D^3 B(\nabla B)}{3 \rho \mu_0} \tag{9}$$

where N is the number of magnetic nanoparticles in each oil droplet, μ_0 is the permeability of empty space, $\Delta \chi$ is the difference in magnetic susceptibility between the magnetic nanoparticles and mineral oil, V_{p} is the volume of a magnetic nanoparticle (m³), B and ∇B are the magnetic flux density (T) and gradient (T/m), respectively, and C and ρ are the concentration and density of the magnetic nanoparticles, respectively. The parameters $\Delta \chi$, C, ρ and μ_0 are fixed for the same magnetic mineral oil and alginate solution. Furthermore, because the conditions used to fabricate magnetic nanoparticles in our experiment were the same as in previous work (Zhang et al. 2009), we consider that the magnetic nanoparticles are saturated in the magnetic field used here. Thus, the magnetic forces are proportional to ∇B for MOMs with the same diameter. Regarding MOMs with different diameters, the magnetic forces are proportional to D^3 at the same ∇B. The magnetic forces acting on the whole microfiber can be calculated by either directly counting the number of MOMs (N_{d}) throughout the microfiber or estimating N_{d}:

$$N_d = \frac{V_{fiber}t_n}{L} \qquad (10)$$

where V_{fiber} is microfiber velocity, which could be measured using the same method as for measuring MOM deflection velocity, and t_n is microfiber spinning time. However, precise control of spinning time should be studied further.

For previous polymer microfiber assemblies deposited under solution conditions, buoyancy prevented the microfibers from attaching to the surface of the substrate, which limited fabrication of complicated 3D assemblies in solution environments (Ghorbanian et al. 2014). This problem can be effectively solved by putting a magnet under the substrate to induce the magnetic microfibers to deposit. Simultaneously, loose microfiber assemblies can be compacted using magnetic forces, as shown in Fig. 6d. The hybrid microfibers produced here show advantages for magnetic microfiber assembly. First, the magnetic nanoparticles are encapsulated into MOMs rather than directly into the alginate microfiber, which may prevent the potentially negative effect of MOMs on the cells encapsulated in the alginate microfibers. Second, the estimated magnetic force acting on the microfibers allows us to calculate the microfiber deposition speed in solution. The microfiber deposition speed can be changed by modifying the concentration of encapsulated MOMs to synchronize with the microfiber spinning speed, which may allow us to fabricate 3D assemblies with uniform alginate microfiber distribution.

The controlled structure and estimated magnetic force of the microfibers may allow selective collection of microfibers at a target location. This selective collection may enable microfibers encapsulating different agents to be released in turn at the same target location. A similar selective collection process has been studied previously (Suh et al. 2012). The magnetic oil solution could be extended to PLGA–DMC solution to produce microfibers that are expected to act as a dual delivery carrier (Yu et al. 2014). The developed method could be used to fabricate hybrid microfibers with desired width, diameter of PLGA–DMC microdroplets and distance between consecutive PLGA–DMC microdroplets. By cutting the microfiber or controlling the spinning time to meet the desired number of encapsulated microdroplets, a size-controlled dual drug microcarrier could be obtained. Controlled size is crucial for drug delivery vehicles to regulate drug release kinetics. Furthermore, the generated size-controlled microcarriers could be improved as a smart drug targeted delivery system with controlled drug release properties by encapsulating magnetic nanoparticles in PLGA solution.

4 Conclusion

In this study, MOMs were successfully encapsulated into alginate microfibers by a microfluidic flow-focusing device with a long gelation microchannel. Use of a long gelation microchannel enabled control of CaCl$_2$ solution flow rate during microfiber fabrication and provided an observation microchannel where we could analyze the effects of the flow rates of oil, alginate and CaCl$_2$ solutions on the fabrication of hybrid microfibers. We developed a hybrid microfiber generation model based on flow rate, which allowed us to produce hybrid microfibers with desired microfiber width, microdroplet diameter and distance between the consecutive microdroplets. A long gelation microchannel also allowed us to measure the magnetic force acting on a single MOM using a magnetic deflection method. We further estimated the magnetic forces acting on a hybrid microfiber by counting the number of encapsulated MOMs. Benefiting from controlled structure and estimated magnetic forces in a specific magnetic field, the generated magnetic hybrid microfibers hold great promise for application in materials science, tissue engineering and regenerative medicine.

References

Agarwal P, Zhao ST, Bielecki P, Rao W, Choi JK, Zhao Y, Yu JH, Zhang WJ, He XM (2013) One-step microfluidic generation of pre-hatching embryo-like core-shell microcapsules for miniaturized 3D culture of pluripotent stem cells. Lab Chip. doi:10.1039/c3lc50678a

Atencia J, Beebe DJ (2005) Controlled microfluidic interfaces. Nature 437:648–655. doi:10.1038/nature04163

Christopher GF, Anna SL (2007) Microfluidic methods for generating continuous droplet streams. J Phys D Appl Phys 40:319–336. doi:10.1088/0022-3727/40/19/R01

Ghorbanian S, Qasaimeh MA, Akbari M, Tamayol A, Juncker D (2014) Microfluidic direct writer with integrated declogging mechanism for fabricating cell-laden hydrogel constructs. Biomed Microdevices. doi:10.1007/s10544-014-9842-8

Hanuš J, Ullrich M, Dohnal J, Singh M, Štěpánek F (2013) Remotely controlled diffusion from magnetic liposome microgels. Langmuir 29:4381−4387. doi.org/10.1021/la4000318

Hu CZ, Nakajima M, Yue T, Takeuchi M, Seki M, Huang Q, Fukuda T (2013) On-chip fabrication of magnetic alginate hydrogel microfibers by multilayered pneumatic microvalves. Microfluid Nanofluidics. doi:10.1007/s10404-013-1325-3

Jose MB, Cubaud T (2012) Droplet arrangement and coalescence in diverging/converging microchannels. Microfluid Nanofluidics 12:687–696. doi:10.1007/s10404-011-0909-z

Kang E, Jeong GS, Choi YY, Lee KH, Khademhosseini A, Lee SH (2011) Digitally tunable physicochemical coding of material

composition and topography in continuous microfibres. Nat Mater 10:877–883. doi:10.1038/NMAT3108

Kang E, Choi YY, Chae SK, Moon JH, Chang JY, Lee SH (2012) Microfluidic spinning of flat alginate fibers with grooves for cell-aligning scaffolds. Adv Mater 24:4271–4277. doi:10.1002/adma.201201232

Lee CB, Chang CC, Huang SB, Yang RJ (2006) The hydrodynamic focusing effect inside rectangular microchannels. J Micromech Microeng 16:1024–1032

Li YH, Huang GY, Zhang XH, Li BQ, Chen YM, Liu TL, Lu TJ, Xu F (2013) Magnetic hydrogels and their potential biomedical applications. Adv Funct Mater 23:660–672. doi:10.1002/adfm.201201708

Lin YS, Huang KS, Yang CH, Wang CY, Yang YS, Hsu HC, Liao YJ, Tsai CW (2012) Microfluidic synthesis of microfibers for magnetic-responsive controlled drug release and cell culture. PLoS One. doi:10.1371/journal.pone.0033184

Liu HH, Zhang YH (2011) Droplet formation in microfluidic cross-junctions. Phys Fluids 23:987–999

Liu J, Shi J, Zhang F, Wang L, Yamamoto S, Takano M, Lianmei J, Haoli Z (2012) Segmented magnetic nanofibers for single cell manipulation. Appl Surf Sci 258:7530–7535. doi:10.1016/j.apsusc.2012.04.077

Miller E, Rotea M, Rothstein JP (2010) Microfluidic device incorporating closed loop feedback control for uniform and tunable production of micro-droplets. Lab Chip 10:1293–1301. doi:10.1039/b925497h

Shin SJ, Park JY, Lee JY, Park H, Park YD, Lee KB, Whang CM, Lee SH (2007) "On the fly" Continuous Generation of alginate fibers using a microfluidic device. Langmuir 23:9104–9108

Suh SK, Chapin SC, Hatton TA, Doyle PS (2012) Synthesis of magnetic hydrogel microparticles for bioassays and tweezer manipulation in microwells. Microfluid Nanofluidics 13:665–674. doi:10.1007/s10404-012-0977-8

Sun RP, Cubaud T (2011) Dissolution of carbon dioxide bubbles and microfluidic multiphase flows. Lab Chip 11:2924–2928. doi:10.1039/c1lc20348g

Thomas A, Gilson CD, Ahmed T (1995) Gelling of alginate fibres. J Chem Technol Biotechnol 64:73–79

Thorsen T, Roberts RW, Arnold FH, Quake SR (2001) Dynamic pattern formation in a vesicle-generating microfluidic device. Phys Rev Lett 86:4163–4166. doi:10.1103/PhysRevLett.86.4163

Vladisavljević GT, Kobayashi I, Nakajima M (2012) Production of uniform droplets using membrane, microchannel and microfluidic emulsification devices. Microfluid Nanofluidics 13:151–178. doi:10.1007/s10404-012-0948-0

Xu F, Wu MCA, Rengarajan V, Finley TD, Keles HO, Sung Y, Li BQ, Gurkan UA, Demirci U (2011) Three-dimensional magnetic assembly of microscale hydrogels. Adv Mater 23:4254–4260. doi:10.1002/adma.201101962

Yamada M, Sugaya S, Naganuma Y, Seki M (2012) Microfluidic synthesis of chemically and physically anisotropic hydrogel microfibers for guided cell growth and networking. Soft Matter 8:3122–3130

Yang K, Peng HB, Wen YH, Li N (2009a) Re-examination of characteristic FTIR spectrum of secondary layer in bilayer oleic acid-coated Fe_3O_4 nanoparticles. Appl Surf Sci 256:3093–3097. doi:10.1016/j.apsusc.2009.11.079

Yang CH, Huang KS, Lin YS, Lu K, Tzeng CC, Wang EC, Lin CH, Hsu WY, Chang JY (2009b) Microfluidic assisted synthesis of multi-functional polycaprolactone microcapsules: incorporation of CdTe quantum dots, Fe_3O_4 superparamagnetic nanoparticles and tamoxifen anticancer drugs. Lab Chip 9:961–965. doi:10.1039/b814952f

Yu Y, Wen H, Ma JY, Lykkemark S, Xu H, Qin JH (2014) Flexible fabrication of biomimetic bamboo-like hybrid microfibers. Adv Mater 26:2494–2499. doi:10.1002/adma.201304974

Zhang K, Liang QL, Ma S, Mu X, Hu P, Wang YM, Luo G (2009) On-chip manipulation of continuous picoliter-volume superparamagnetic dorplets using a magnetic force. Lab Chip 9:2992–2999